Research Article | Vol. 12, No. 9 / 1 Sep 2021 / Biomedical Optics Express 5909
Biomedical Optics EXPRESS

Two-photon peak molecular brightness spectra reveal long-wavelength enhancements of multiplexed imaging depth and photostability

RYAN T. LANG[1,2] AND BRYAN Q. SPRING[1,2,3,*]

[1]Translational Biophotonics Cluster, Northeastern University, Boston, MA 02115, USA
[2]Department of Physics, Northeastern University, Boston, MA 02115, USA
[3]Department of Bioengineering, Northeastern University, Boston, MA 02115, USA
[*]b.spring@northeastern.edu

Abstract: The broad use of two-photon microscopy has been enabled in part by Ti:Sapphire femtosecond lasers, which offer a wavelength-tunable source of pulsed excitation. Action spectra have thus been primarily reported for the tunable range of Ti:Sapphire lasers (~700–1000 nm). However, longer wavelengths offer deeper imaging in tissue via reduced scattering and spectral dips in water absorption, and new generations of pulsed lasers offer wider tunable ranges. We present the peak molecular brightness spectra for eight Alexa Fluor dyes between 700–1300 nm as a first-order surrogate for action spectra measured with an unmodified commercial microscope, which reveal overlapping long-wavelength excitation peaks with potential for multiplexed excitation. We demonstrate simultaneous single-wavelength excitation of six spectrally overlapping fluorophores using either short (~790 nm) or long (~1090 nm) wavelengths, and that the newly characterized excitation peaks measured past 1000 nm offer improved photostability and enhanced fidelity of linear spectral unmixing at depth compared to shorter wavelengths.

1. Introduction

Multiphoton excited fluorescence, wherein a fluorophore is excited to a higher electronic energy state by the simultaneous absorption of two or more photons, is one of the most broadly utilized applications of nonlinear optics to biology [1,2]. Two-photon excitation (TPE) microscopy provides several well-known advantages over conventional microscopy, including intrinsic optical sectioning [3], reduced scattering and absorption of excitation light [4], and superior imaging at depth [5]. TPE spectra frequently have multiple peaks whose features are partially determined by vibronic transitions. Centrosymmetric or nearly-centrosymmetric molecules [6] exhibit moderate broadening relative to single-photon excitation (or one-photon excitation, OPE) due to parity selection rules [7]. This can be exploited to enhance simultaneous excitation of multiple fluorophores (*i.e.* multiplexing), as demonstrated by the seminal work of Xu and colleagues [8]. However, multiplexing TPE has been relatively underdeveloped since then, perhaps due in part to the lack of commercial hyperspectral TPE microscopes until the past few years. Recently, Bares *et al.* elegantly developed the use of multiple femtosecond lasers (three different excitation wavelengths) in combination with angle-tuned spectral filters to image up to 10 different spectrally overlapped fluorescent probes at depth *in vivo* [9]. Simultaneous excitation has also been improved by employing wavelength mixing schemes, where pulse train synchronization of multiple wavelengths creates additional virtual excitation energies [10].

In general, predicting optimal TPE wavelengths by simply doubling one-photon excitation (OPE) spectra is not reliable due to nonlinear broadening and blue-shifting effects [11,12], necessitating measurements of two-photon absorption (TPA) cross-sections. Collections of measurements such as Makarov *et al.* [13] indicate that independent measurements of TPA cross-sections can vary significantly. The peak molecular brightness has been introduced as a

#433989 https://doi.org/10.1364/BOE.433989
Journal © 2021 Received 11 Jun 2021; revised 23 Aug 2021; accepted 24 Aug 2021; published 1 Sep 2021

Biomedical Optics EXPRESS

viable alternative measurement to the TPA cross-section [14–17]. Iyer *et al.* [16] thoroughly investigated the use of two-photon fluorescence correlation spectroscopy (FCS) to investigate the molecular brightness ε. At low laser powers, ε has a squared dependence on the excitation intensity; however, higher-order bleaching and saturation effects dominate at high powers and reduce ε. Due to these competing effects ε reaches a peak value ε_{max} that conveys fluorescence intensity and photostability information. This relies on the fact that photobleaching is dominant over saturation effects at ε_{max}, which might not be the case for highly photostable chromophores. The spectral response of ε_{max} has been shown to be highly repeatable for organic dyes used in the life sciences [16], and the measurement is considerably simpler than TPA cross-section measurements.

Mütze *et al.* [17] has reported the spectra of ε_{max} versus excitation wavelength for a wide range of fluorophores over the tunable range of a Ti:Sapphire laser (approx. 700-1000 nm). As tunable laser ranges expand, multiphoton signatures should be extended to include previously identified long-wavelength windows for deep tissue imaging [18,19]. In particular, data presented by Mütze suggests that many of the commonly used Alexa Fluor dyes may exhibit significant TPE ε_{max} peaks beyond 1000 nm. Longer wavelengths have been shown to offer deeper imaging capabilities [19] and significantly reduced photobleaching effects [20]. Increased water absorption can also be mitigated through strategic selection of excitation wavelengths to access dips in the water absorption spectrum [21]; for example, Horton *et al.* optimized three-photon excitation at 1700 nm in part by considering the contribution of water absorption to signal attenuation [22].

Although broader spectra [7] of TPE allow for greater simultaneous fluorophore excitation than OPE [23], basic filter-based microscopy is generally limited to three or four fluorophores. Multiplexing is generally undesirable for filter-based microscopy due to channel cross-talk and the inability to decompose the spectral contributions. Hyperspectral multiplexing overcomes this limitation by measuring the simultaneous signal of spectrally overlapping dyes on a continuum of spectral detectors [24–26] and resolving the relative abundances through various unmixing methods [27–29], albeit with a relative loss in signal-to-noise due to dispersing the emitted photons into spectral bins. While recent developments utilize several TPE wavelengths to excite dye panels [9,10], a single TPE wavelength is capable of simultaneously exciting multiple dyes itself. Single-wavelength OPE multiplexing has been demonstrated by engineering probe mutants with elongated stokes shifts [30], whereas TPE enables the use of commercially available dyes for similar results.

Previous demonstrations of single-wavelength TPE hyperspectral multiplexing have multiplexed intrinsic [31–34] and extrinsic [35,36] fluorophores, achieving simultaneous excitation of up to four fluorophores with overlapping emission spectra signatures (endmembers). Herein, we present the peak molecular brightness spectra for eight Alexa Fluor dyes, which are used broadly in life sciences publications and are already well-characterized with known chemical structure and spectroscopic properties [37,38]. Using an unmodified commercial microscope, we extend previous measurements to 1300 nm and revealing distinct TPE peaks past 1000 nm. The measured spectra were used to predict optimal TPE wavelengths for simultaneous fluorophore excitation. Additionally, the molecular brightness method was extended to quantitatively predict wavelength-dependent photobleaching half-life. Tissue phantoms were engineered following previous reports [19,39] to mimic the effects of excitation light scattering when imaging at depth. We demonstrate accurate unmixing of six spectrally overlapping fluorophores using a single excitation wavelength, and also show that longer TPE wavelengths retain higher unmixing fidelity at depth and with enhanced photostability.

Biomedical Optics EXPRESS

2. Materials and methods

2.1. Peak molecular brightness measurement

An unmodified commercial microscope (LSM 880, Zeiss) with a nonlinear excitation module was configured to measure the spectrum of ε_{max} versus wavelength (Fig. 1(a); for additional details, see Supplement 1 Section A). An InSightX3 DUAL-AX pulse laser was used in the microscope's FCS mode to excite dye samples, whose fluorescence was recorded on the 32 channel "Quasar" GaAsP PMT in photon counting mode. Experiments were carried out using a 40x, 1.2 NA water-immersion objective (C-Apochromat 40x/1.20 W Corr M27, Zeiss). For all nonlinear excitation experiments, the pinhole was opened to the maximum extent possible to maximize signal. We observed a maximum of 160-200 dark counts per second when using all 32 channels, while signal levels were at least 5-10 kilocounts per second. The dynamic detection range of the PMT (total range: 400-700 nm) was set to match each dye's emission signature to further limit dark counts. FCS autocorrelation curves were calculated with the ZEN 2.3 (Black) FCS module.

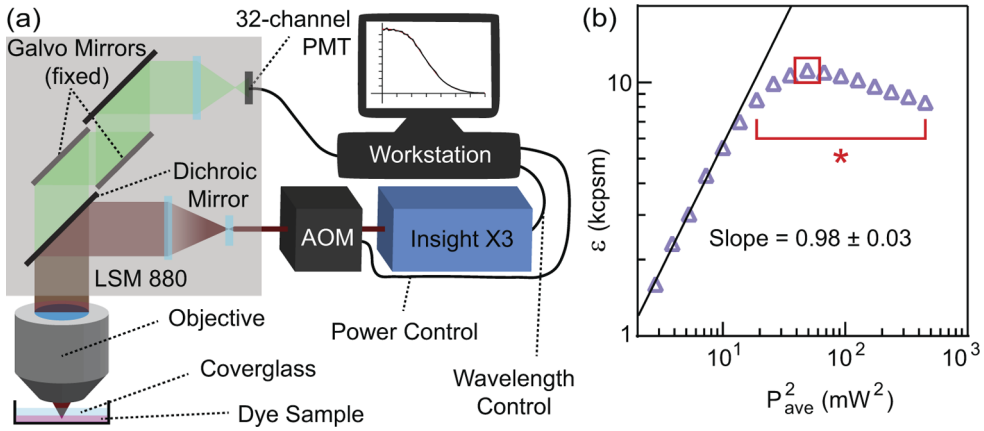

Fig. 1. (a) Setup to use a commercial microscope (Zeiss LSM 880) to measure molecular brightness of fluorophore dye samples based on fluorescence correlation spectroscopy. Key microscope components for this experiment are labeled; spectral grating, scanhead not shown. PMT, photomultiplier tube; AOM, acousto-optic modulator. (b) The molecular brightness is linearly dependent on the square of the laser power (quadratic dependence) at low powers, which is eventually dominated by bleaching and saturation effects (*, red bracket), creating a peak in the molecular brightness (red square).

Eight Alexa Fluor dyes were examined in the present study: Alexa Fluor 488 (A37570, ThermoFisher; abbreviated, *e.g.*, A488), Alexa Fluor 514 (A30002, ThermoFisher), Alexa Fluor 532 (1041-1, Fluoroprobes), Alexa Fluor 546 (A20002, ThermoFisher), Alexa Fluor 568 (1081-1, Fluoroprobes), Alexa Fluor 594 (1101-1, Fluoroprobes), Alexa Fluor 610 (A30050, ThermoFisher), and Alexa Fluor 633 (A20005, ThermoFisher). Dye solutions were prepared in DI H_2O to avoid fluorescence quenching effects from pH buffers [17]. The pH was measured with an electrode sensor (13-643-133, ThermoFisher) and found to be well within the stable range specified by the manufacturer (see Supplement 1 Table S1). Dye solutions were prepared between 1-10 nM immediately before measurement; concentrations of each dye were fine-tuned to ensure adequate emission signal. These concentrations are well below the micromolar threshold at which aggregates and dimers form for Alexa Fluor dyes [40]. The tunable range of the InSightX3 (680–1000, 1080–1300 nm) was scanned in 10 nm steps, starting at 710 nm to avoid the 400–700 nm detection range of the PMT. The idler beam provided an additional data point at 1045 nm. At

Biomedical Optics EXPRESS

each wavelength, the laser power was modulated in 15 logarithmically spaced steps. At each power setting, photons were collected for 45-90 seconds, longer for lower fluorescence intensity.

The molecular brightness ε, while typically described in relation to TPE action cross section (see Supplement 1 Section B), can be calculated directly from the fluorescence correlation amplitude $G(0)$, and fluorescence intensity $\langle F(t)\rangle$ as $\varepsilon = \langle F(t)\rangle G(0) = \langle F(t)\rangle / N_{AC}$, where $N_{AC} = 1/G(0)$ is the mean number of molecules as determined by the autocorrelation function. However, to ensure consistency the correlation curve was fit to a standard model for three dimensional free diffusion [41] using the ZEN FCS software:

$$G(\tau) = \frac{G(0)}{(1 + \tau/\tau_d)(1 + k^{-2}\tau/\tau_d)^{1/2}} \tag{1}$$

where τ_d is the diffusion time and k is the form factor (ratio of axial over lateral radius of the focal volume), although only $G(0)$ was of interest in this study. No triplet state dynamics were included after analyzing Chi-square fits for simple diffusion and triplet fits, in agreement with similar past studies [16,17]. After determination of ε, data was analyzed and plotted using Microsoft Excel and GraphPad Prism.

Laser power throughput and stability was characterized independently as it could not be simultaneously monitored. The laser power delivered to the sample at maximum power was measured in 10 nm steps, and the linearity of the acousto-optic modulator was confirmed as well for the powers described above in steps of 100 nm (see Supplement 1 Fig. S1); both measurements were made in the sample plane using a power meter (PM100D, Thorlabs) and compatible power meter sensor (S130C, Thorlabs) with the beam parked in a stationary mode.

2.2. Photobleaching half-life

The photobleaching of six fluorophores (A532, A546, A568, A594, A610, A633) was measured at 790 nm and 1090 nm excitation at 75 mW average excitation power, in a similar method to that of Orth and colleagues [42]. First, epithelial cells (NIH:OVCAR5) were prepared as stained contrast agents. Cells were fixed with 4% paraformaldehyde (19943 1 LT, Affymetrix), quenched with 0.1 M glycine (G46-500, Fisher) and permeabilized with 0.1% v/v TritonX-100 (BP151-100, Fisher). Cells were then stained with Alexa Fluor NHS esters in 0.1 M sodium bicarbonate (25080094, Thermofisher), which bind protein amine groups to stain the cells. Slides were prepared and imaged continuously in selected positions to measure fluorescence decrease due to signal. At every frame, a 32-channel spectral image cube (x, y, λ) was obtained with a near-IR long working distance objective (W Plan-Apochromat 20x/1.0 DIC (UV) VIS-IR M27; Zeiss).

Spectral image cubes were also taken of control slides of cells stained with each fluorophore, from which dye emission spectra were extracted. All spectral image cubes were linearly unmixed using a parallelized non-negative least squares algorithm to determine the abundance of each dye at every pixel. The average signal in each frame was normalized and plotted, and bleaching half-life was extracted as the frame at which the intensity had decreased by 50%. Independently, a prediction of the relative half-lives of the six fluorophores at both wavelengths was calculated from molecular brightness measurements described earlier (see Supplement 1 Section C). The Pearson's correlation coefficient was calculated between the predicted and measured relative half-lives.

2.3. Hyperspectral multiplexing in a tissue phantom

A tissue phantom was created to mimic the effects of scattering and water absorption in TPE imaging at depth. Cells were prepared as contrast agents as described in the previous section. Two panels of stains were created; one panel of six single-stain cells (A532, A546, A568, A594, A610, A633; single-dye panel) and one panel of cells stained with both A546 and A568 at two different relative concentrations (3:1 A546:A568 and 1:3 A546:A568; mix-dye panel). Two

Biomedical Optics EXPRESS

tissue phantoms (one for each dye panel) were prepared by mixing low-melt agarose (A9414-10G, Sigma-Aldrich) at 1.0% v/v in phosphate-buffered saline (10010023, ThermoFisher) to capture water absorption, 1-μm diameter polystyrene beads (100181, PolyScience) at $2.7 \cdot 10^9$ beads/mL as scattering agents, and a panel of stained cells at approximately $6 \cdot 10^6$ cells/mL.

Phantom imaging was carried out using the same commercial microscope and laser as described in the previous section. Lateral 32-channel spectral image cubes (x, y, λ as Z-slices) were obtained at 2 μm increments from the surface to a depth of 600 μm. Imaging was carried out using TPE wavelengths of 790 nm and 1090 nm, which were selected from the peak molecular brightness results, in five randomly selected XY positions in each phantom.

Unmixing was performed as described in the previous section. Unmixing error to signal ratio was calculated using a custom MATLAB (Mathworks) program (see Supplement 1 Section D) and plotted versus z-depth to compare the two excitation wavelengths. The data was fit to $\delta = be^{z/a} - c$, where c and b were shared parameters between the two TPE wavelengths so that a represented a characteristic attenuation length of δ. Data was analyzed and plotted using GraphPad Prism for all analysis described herein.

3. Results and discussion

3.1. Peak molecular brightness measurement

Peak molecular brightness has been shown to offer a measurement of spectral fluorescence activity [16] as a first order approximation of the TPE action spectra. While absolute photon counts are setup-specific, the relative spectral-shape profile of the spectral response - which is often sufficient for multiplexed experiment design - is intrinsically robust and reproducible among different setups (see Supplement 1 Table S2). For this molecular brightness measurement, the two-photon spectral shape is independent of dye concentration, pulse train characteristics, wavelength dependent laser transmittance, and detection efficiency. Therefore, the ease of measurement of the molecular brightness may make it attractive for certain applications. In contrast, the two-photon cross-section measurement is the gold standard for quantifying the two photon excitation spectrum in Goeppert-Meyer units.

While a diffusion model was used here to ensure accurate $G(0)$ calculation, these values did not differ significantly from those directly calculated from the autocorrelation function. Triplet state dynamics, which necessitate additional fitting terms to accurately calculate $G(0)$, are integral in photobleaching processes for one-photon excitation. However, TPE FCS does not involve triplet state dynamics, even at high powers that cause significant photobleaching [43,44]. Adding triplet terms did not improve the chi-square of the fit significantly, so it was not included (see Supplement 1 Fig. S2).

We present peak molecular brightness spectra for eight Alexa Fluor dyes (Fig. 2). The brightest dye, A546, shows a peak ε_{max} value of 19 kilocounts per second per molecule (kcpsm). This is similar to a reported value of 15.0 kcpsm by Iyer *et al.* for A546 using a similar setup and a GaAsP PMT [16]. Iyer reports a 2.3-fold increase by using an APD due to higher quantum efficiency, which was further improved by Mütze *et al.* to 58 kcpsm with even more sensitive equipment [17]. We leave this difference uncorrected as it may inform relative brightness using a PMT during standard microscopy. The measured peak molecular brightness is not consistent between experimental setups since it is directly proportional to the photon collection efficiency and the laser intensity squared. For example, relative signal here is diminished for the redder dyes (A610, A633) due to the falloff in detection efficiency for GaAsP PMTs versus APDs in this range. However, spectral variation (*i.e.* the shape of the curve) of peak molecular brightness is chiefly of interest and is intrinsically consistent across experimental setups. The overlapping portions of the spectra shown here with those in Mütze *et al.* have Pearson's correlation coefficients between 0.943 and 0.993 (see Supplement 1 Table S2), demonstrating robust repeatability of this measurement.

Biomedical Optics EXPRESS

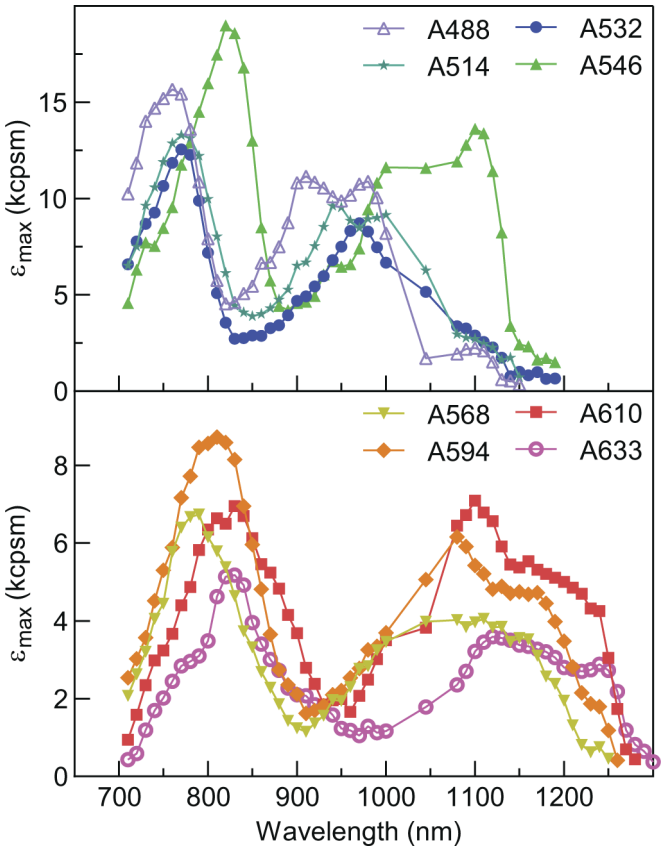

Fig. 2. Peak two-photon excitation molecular brightness spectra for eight Alexa Fluor dyes in DI H_2O. Data in kilocounts per second per molecule (kcpsm) every 10 nm with a line added to connect data points.

All eight dyes have two distinct spectral peaks in their lineshapes, which is a common feature of TPE spectra and has been observed in many other chromophores [23,45,46]. For several dyes (A546, A568, A594, A610, A633), new peaks past 1000 nm (between 1000-1120 nm) were revealed, that, to the best of our knowledge, are not currently reported in the literature. For the other dyes (A488, A514, A532), the secondary peak (between 900-1050 nm) was fully explored and matches existing literature [17]. A characteristic power squared dependence of intensity was confirmed for all sixteen peaks(see Supplement 1 Fig. S2 and Supplement 1 Table S3). The signal is not presented past 1180-1270 nm, depending on the dye, for which insufficient laser power and cross section inhibited accurate determination of ε_{max}.

3.2. Photobleaching half-life

The ratio of the peak molecular brightness and the TPE action cross-section $\varepsilon_{max}/\sigma_2\eta_2$ has been shown to predict photostability [17]. With careful measurements of ε in the low laser power regime, it is possible to calculate $\sigma_2\eta_2$ [17] (see Supplement 1 Section B). Here, the relative photostability was predicted by assuming the laser pulse characteristics to be constant (see Supplement 1 Section C). Using this method, predictions for the relative photobleaching half-life were made (see Supplement 1 Table S4).

The photobleaching response was independently measured and plotted, from which characteristic half-lives were extracted. When normalized, these values match closely to the predicted

Biomedical Optics EXPRESS

values (Fig. 3) with a Pearson's correlation of $\rho = 0.98$. Visual inspection shows that relative half-life trends not only predict wavelength dependent bleaching, but can also predict relative photostability among different fluorophores. The predicted and measured photobleaching half-lives at 790 nm versus 1090 nm clearly favor the longer wavelength, which agrees with previous studies [20]. Additionally, we find that A532 and A546 generally offer greater photostability at these wavelengths than the other dyes. The accurate prediction of relative bleaching half-life demonstrates the useful utility of molecular brightness measurements to inform photostability as well as fluorescence intensity.

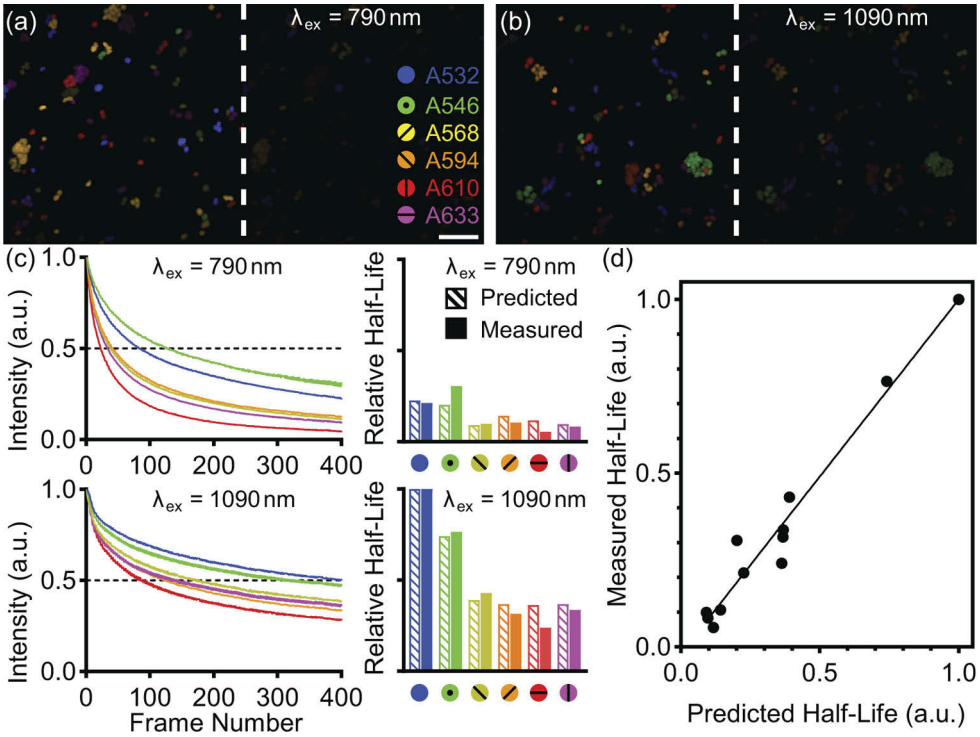

Fig. 3. (a) Unmixed images of single-dye panel showing initial intensity (left) and intensity after 400 frames (right) with 790 nm excitation at 75 mW. (b) A similar depiction repeating the experiment at 1090 nm. (c) Plots of relative fluorescence intensity versus frame number (left) show faster bleaching at 790 nm versus 1090 nm. Bleaching half-life, intersection of curve(s) with dotted line. Predicted relative bleaching half-life from molecular brightness analysis and measured relative half-life for the various fluorophores and TPE short and long wavelengths. (d) Predicted half-life correlates well with measured half-life ($\rho = 0.98$, $P<0.0001$).

3.3. *Hyperspectral multiplexing in a tissue phantom*

We demonstrate simultaneous excitation of six fluorophores (A532, A546, A568, A594, A610, A633) with both 790 nm and 1090 nm TPE (see Supplement 1 Figs. S4, S5). At zero depth, these six fluorophores can be isolated using linear unmixing despite a high degree of spectral overlap. Cells stained with multiple dyes at different staining ratios can also be linearly unmixed to correctly identify the amount of fluorophore signal in each staining ratio. As depth increases, visible and identifiable cells become rarer as fluorescent signal becomes weaker. As the unmixing error to signal ratio δ becomes greater than 1.0 visible cell density falls and the remaining cells

Biomedical Optics EXPRESS

become harder to correctly identify. The last identifiable cells are found around δ of 1.5 to 2.0 for these phantoms. For both excitation wavelengths, all visible cells can be reliably identified up to ~350 μm. Cells may be found and identified between ~350 – 450 μm, but typically only when excited at 1090 nm.

The single-dye panel phantom and the mix-dye panel phantom both exhibited expected behavior of imaging *vs* depth. Raw image signal decreased exponentially with depth, although the decrease was sharper than expected due to Mie scattering from the polystyrene beads. A mean free path (MFP) of 290 µm at 790 nm and 527 µm at 1090 nm was calculated from Mie theory [47], but signal was extinguished by 600 µm in all cases. This can be attributed to the additional geometric scattering and absorption of the stained cells, which is not expected to have a significant wavelength dependence as the objects (cells, 15 µm diameter) are much larger than the wavelengths of excitation and emitted light. We estimate the contribution of cell scattering alone to have an MFP of about 400 µm for both wavelengths, resulting in effective MFPs of 170

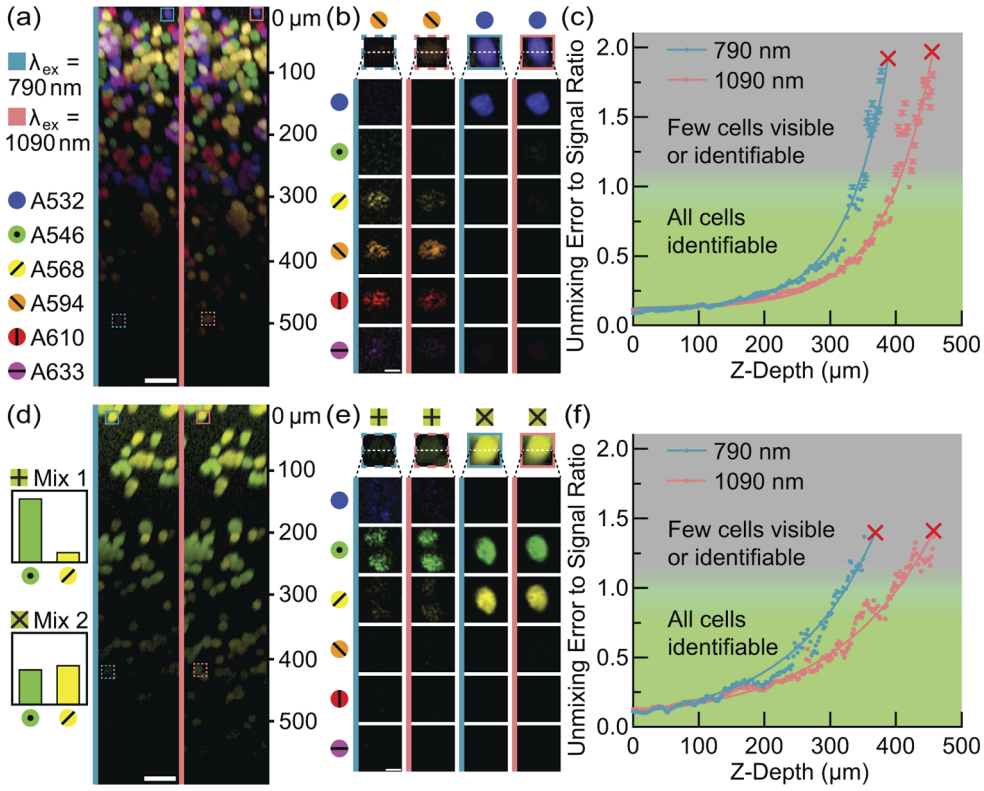

Fig. 4. (a) Unmixed composite XZ images (log of intensity) of the single-dye panel indicate improved imaging depth for λ_{ex} = 1090 nm vs. 790 nm. Scale bar, 50 µm. (b) XY close-ups of selected cells at depth and at the surface visually show improved unmixing fidelity for 1090 nm at depth while there is no significant difference at the surface. Scale bar, 10 µm. (c) Unmixing error to signal ratio increases with image depth and reveals a quantitative advantage of 1090 nm vs. 790 nm for the single-dye panel. Best fit lines are $\delta = be^{a/z} - c$; $a_{1090} > a_{790}$, $P < 0.0001$, c and b are equal for both fits. Red × symbols represent point at which no cells are identifiable. (d-f) Similar results are found for the mix-dye panel, for which λ_{ex} = 1090 nm yields improved imaging depth, visually improved unmixing fidelity of cells at depth and a similar quantitative advantage of 1090 nm *vs.* 790 nm; $a_{1090} > a_{790}$, $P < 0.0001$, c and b are equal for both fits.

Biomedical Optics EXPRESS

μm and 230 μm for 790 nm and 1090 nm, respectively. These values match much more closely to what was found experimentally.

Using excitation light at 1090 nm offers a clear advantage over 790 nm, allowing for deeper imaging depth and lower δ at depth (Fig. 4). For the six single-dye panel phantom, the fit line $\delta = be^{a/z} - c$ found $a_{1090} = 74$ μm and $a_{790} = 63$ μm ($P<0.0001$). For the mix-dye panel phantom, we found $a_{1090} = 152$ μm and $a_{790} = 122$ μm ($P<0.0001$). The differences in a between the two panels are due to the definition of δ; the mix-dye panel only has two possible ground truth cell types, while the single-dye panel has six. This increases unmixing error for the single-dye panel *vs.* the mix-dye panel, so while the a parameter is somewhat arbitrary, it is still useful to compare excitation wavelengths within a panel.

4. Conclusion

The peak molecular brightness spectra of two-photon excited probes have been determined by FCS using a commercial microscope. Eight Alexa Fluor dyes have been measured in the tunable range of an InSightX3 laser (700-1300 nm), extending past the usual Ti:Sapphire range. These spectra revealed two distinct peaks for each fluorophore; one between 700-900 nm and one between 900-1200 nm. Using peak molecular brightness as a first-order surrogate for two-photon action spectra, one wavelength was selected to excite each peak simultaneously (790 nm and 1090 nm) and hyperspectral unmixing of six probes with overlapping emission spectra. The photostability was predicted from molecular brightness analysis at these wavelengths for six probes, predicting better photostability at 1090 nm than 790 nm. This was confirmed by direct measurement of photobleaching half-life for these parameters. Simultaneous probe excitation and linear unmixing was demonstrated for six fluorophores in a tissue phantom. Using stained cells as contrast agents, the unmixing fidelity was calculated and plotted *vs.* depth, revealing that 1090 nm excitation performs offers lower unmixing error at depth than 790 nm. These results offer a guide for wavelength and fluorophore selection for multiplexed two-photon imaging applications.

Funding. Richard and Susan Smith Family Foundation (Smith Family Award); National Institutes of Health (K22 CA181611, R01 CA226855).

Acknowledgments. We thank Robert S. Knox and Chris Xu for preliminary critical discussions regarding single-wavelength multiplexed TPE that encouraged this work. We also thank Guoxin Wong and the Institute for Chemical Imaging of Living Systems at Northeastern University for consultation and imaging support.

Disclosures. The authors declare no conflicts of interest.

Data Availability. Data used to produce the images and graphs in this paper are not publicly hosted for download due to large file sizes but may be obtained from the authors upon reasonable request.

Supplemental document. See Supplement 1 for supporting content.

References

1. P. T. So, E. Y. Yew, and C. Rowlands, "High-throughput nonlinear optical microscopy," Biophys. J. **105**(12), 2641–2654 (2013).
2. W. R. Zipfel, R. M. Williams, and W. W. Webb, "Nonlinear magic: Multiphoton microscopy in the biosciences," Nat. Biotechnol. **21**(11), 1369–1377 (2003).
3. W. Denk, J. H. Strickler, and W. W. Webb, "Two-photon laser scanning fluorescence microscopy," Science **248**(4951), 73–76 (1990).
4. C. Ash, M. Dubec, K. Donne, and T. Bashford, "Effect of wavelength and beam width on penetration in light-tissue interaction using computational methods," Lasers Med. Sci. **32**(8), 1909–1918 (2017).
5. A. M. Smith, M. C. Mancini, and S. Nie, "Bioimaging: Second window for in vivo imaging," Nat. Nanotechnol. **4**(11), 710–711 (2009).
6. N. S. Makarov, M. Drobizhev, G. Wicks, E. A. Makarova, E. A. Lukyanets, and A. Rebane, "Alternative selection rules for one- and two-photon transitions in tribenzotetraazachlorin: Quasi-centrosymmetrical π-conjugation pathway of formally non-centrosymmetrical molecule," J. Chem. Phys. **138**(21), 214314 (2013).
7. C. Xu and W. W. Webb, "Measurement of two-photon excitation cross sections of molecular fluorophores with data from 690 to 1050 nm," J. Opt. Soc. Am. B **13**(3), 481 (1996).

Biomedical Optics EXPRESS

8. C. Xu, W. Zipfel, J. B. Shear, R. M. Williams, and W. W. Webb, "Multiphoton fluorescence excitation: New spectral windows for biological nonlinear microscopy," Proc. Natl. Acad. Sci. U. S. A. **93**(20), 10763–10768 (1996).
9. A. J. Bares, M. A. Mejooli, M. A. Pender, S. A. Leddon, S. Tilley, K. Lin, J. Dong, M. Kim, D. J. Fowell, N. Nishimura, and C. B. Schaffer, "Hyperspectral multiphoton microscopy for in vivo visualization of multiple, spectrally overlapped fluorescent labels," Optica **7**(11), 1587 (2020).
10. P. Mahou, M. Zimmerley, K. Loulier, K. S. Matho, G. Labroille, X. Morin, W. Supatto, J. Livet, D. Débarre, and E. Beaurepaire, "Multicolor two-photon tissue imaging by wavelength mixing," Nat. Methods **9**(8), 815–818 (2012).
11. C. Xu, R. M. Williams, W. Zipfel, and W. W. Webb, "Multiphoton excitation cross-sections of molecular fluorophores," Bioimaging **4**(3), 198–207 (1996).
12. F. Bestvater, E. Spiess, G. Stobrawa, M. Hacker, T. Feurer, T. Porwol, U. Berchner-Pfannschmidt, C. Wotzlaw, and H. Acker, "Two-photon fluorescence absorption and emission spectra of dyes relevant for cell imaging," J. Microsc. **208**(2), 108–115 (2002).
13. N. S. Makarov, M. Drobizhev, and A. Rebane, "Two-photon absorption standards in the 550-1600 nm excitation wavelength range," Opt. Express **16**(6), 4029 (2008).
14. K. G. Heinze, A. Koltermann, and P. Schwille, "Simultaneous two-photon excitation of distinct labels for dual-color fluorescence crosscorrelation analysis," Proc. Natl. Acad. Sci. U. S. A. **97**(19), 10377–10382 (2000).
15. D. R. Larson, W. R. Zipfel, R. M. Williams, S. W. Clark, M. P. Bruchez, F. W. Wise, and W. W. Webb, "Water-soluble quantum dots for multiphoton fluorescence imaging in vivo," Science **300**(5624), 1434–1436 (2003).
16. V. Iyer, M. J. Rossow, and M. N. Waxham, "Peak two-photon molecular brightness of fluorophores is a robust measure of quantum efficiency and photostability," J. Opt. Soc. Am. B **23**(7), 1420 (2006).
17. J. Mütze, V. Iyer, J. J. MacKlin, J. Colonell, B. Karsh, Z. Petrášek, P. Schwille, L. L. Looger, L. D. Lavis, and T. D. Harris, "Excitation spectra and brightness optimization of two-photon excited probes," Biophys. J. **102**(4), 934–944 (2012).
18. J. P. Ritz, A. Roggan, C. Isbert, G. Mller, H. J. Buhr, and C. T. Germer, "Optical properties of native and coagulated porcine liver tissue between 400 and 2400 nm," Lasers Surg. Med. **29**(3), 205–212 (2001).
19. D. Kobat, M. E. Durst, N. Nishimura, A. W. Wong, C. B. Schaffer, and C. Xu, "Deep tissue multiphoton microscopy using longer wavelength excitation," Opt. Express **17**(16), 13354 (2009).
20. V. Andresen, S. Alexander, W. M. Heupel, M. Hirschberg, R. M. Hoffman, and P. Friedl, "Infrared multiphoton microscopy: subcellular-resolved deep tissue imaging," Curr. Opin. Biotechnol. **20**(1), 54–62 (2009).
21. K. Jansen, M. Wu, A. F. Van der Steen, and G. Van Soest, "Photoacoustic imaging of human coronary atherosclerosis in two spectral bands," Photoacoustics **2**(1), 12–20 (2014).
22. N. G. Horton, K. Wang, D. Kobat, C. G. Clark, F. W. Wise, C. B. Schaffer, and C. Xu, "In vivo three-photon microscopy of subcortical structures within an intact mouse brain," Nat. Photonics **7**(3), 205–209 (2013).
23. M. Yamanaka, K. Saito, N. I. Smith, Y. Arai, K. Uegaki, Y. Yonemaru, K. Mochizuki, S. Kawata, T. Nagai, and K. Fujitaa, "Visible-wavelength two-photon excitation microscopy for fluorescent protein imaging," J. Biomed. Opt. **20**(10), 1 (2015).
24. R. A. Schultz, T. Nielsen, J. R. Zavaleta, R. Ruch, R. Wyatt, and H. R. Garner, "Hyperspectral Imaging: A Novel Approach for Microscopic Analysis," Cytometry **43**(4), 239–247 (2001).
25. G. Lu and B. Fei, "Medical hyperspectral imaging: a review," J. Biomed. Opt. **19**(1), 010901 (2014).
26. L. Gao and R. T. Smith, "Optical hyperspectral imaging in microscopy and spectroscopy - A review of data acquisition," J. Biophotonics **8**(6), 441–456 (2015).
27. N. Keshava, "A Survey of Spectral Unmixing Algorithms," Lincoln Laboratory Journal **14**, 55–78 (2003).
28. F. Cutrale, V. Trivedi, L. A. Trinh, C. L. Chiu, J. M. Choi, M. S. Artiga, and S. E. Fraser, "Hyperspectral phasor analysis enables multiplexed 5D in vivo imaging," Nat. Methods **14**(2), 149–152 (2017).
29. E. M. Kercher, J. Tatz, A. Palanisami, Q. Fang, and B. Q. Spring, "Video-rate hyperspectral unmixing for multiplexed molecular microscopy and microendoscopy," Scientific Reports (to be published).
30. A. M. Bittel, A. M. Davis, L. Wang, M. A. Nederlof, J. O. Escobedo, R. M. Strongin, and S. L. Gibbs, "Varied Length Stokes Shift BODIPY-Based Fluorophores for Multicolor Microscopy," Sci. Rep. **8**(1), 4590–4612 (2018).
31. A. J. Radosevich, M. B. Bouchard, S. A. Burgess, R. Stolper, B. Chen, and E. M. Hillman, "Hyperspectral in vivo two-photon microscopy of intrinsic contrast," Opt. Lett. **33**(18), 2164–2166 (2008).
32. L. E. Grosberg, A. J. Radosevich, S. Asfaha, T. C. Wang, and E. M. Hillman, "Spectral characterization and unmixing of intrinsic contrast in intact normal and diseased gastric tissues using hyperspectral two-photon microscopy," PLoS One **6**(5), e19925 (2011).
33. Y. Liu, H. Tu, S. You, E. J. Chaney, M. Marjanovic, and S. A. Boppart, "Label-free molecular profiling for identification of biomarkers in carcinogenesis using multimodal multiphoton imaging," Quant. Imaging Medicine Surg. **9**(5), 742 (2019).
34. S. You, R. Barkalifa, E. J. Chaney, H. Tu, J. Park, J. E. Sorrells, Y. Sun, Y. Z. Liu, L. Yang, D. Z. Chen, M. Marjanovic, S. Sinha, and S. A. Boppart, "Label-free visualization and characterization of extracellular vesicles in breast cancer," Proc. Natl. Acad. Sci. U. S. A. **116**(48), 24012–24018 (2019).
35. S.-Y. Chen, C.-S. Lu, and C.-H. Yeh, "Non-de-scanned parallel recording two-photon hyperspectral microscopy with high spectral and spatial resolution," Biomed. Opt. Express **5**(2), 338 (2014).
36. F. Deng, C. Ding, J. C. Martin, N. M. Scarborough, Z. Song, G. S. Eakins, and G. J. Simpson, "Spatial-spectral multiplexing for hyperspectral multiphoton fluorescence imaging," Opt. Express **25**(26), 32243 (2017).

Biomedical Optics EXPRESS

37. N. Panchuk-Voloshina, R. P. Haugland, J. Bishop-Stewart, M. K. Bhalgat, P. J. Millard, F. Mao, W.-Y. Leung, and R. P. Haugland, "Alexa Dyes, a Series of New Fluorescent Dyes that Yield Exceptionally Bright, Photostable Conjugates," J. Histochem. Cytochem. **47**(9), 1179–1188 (1999).
38. R. W. Sabnis, *Alexa Fluor Dyes* (John Wiley & Sons, Ltd, 2015), chap. 7-12, pp. 20–34.
39. N. J. Durr, C. T. Weisspfennig, B. A. Holfeld, and A. Ben-Yakar, "Maximum imaging depth of two-photon autofluorescence microscopy in epithelial tissues," J. Biomed. Opt. **16**(2), 026008 (2011).
40. C. K. Johnson and M. Levitus, *Spectroscopy and dynamics of single molecules: Methods and applications* (Elsevier, 2019), chap. 1.6.1 Rhodamines and carborhodamines.
41. J. Mütze, T. Ohrt, and P. Schwille, "Fluorescence correlation spectroscopy in vivo," Laser Photonics Rev. **5**(1), 52–67 (2011).
42. A. Orth, R. N. Ghosh, E. R. Wilson, T. Doughney, H. Brown, P. Reineck, J. G. Thompson, and B. C. Gibson, "Super-multiplexed fluorescence microscopy via photostability contrast," Biomed. Opt. Express **9**(7), 2943 (2018).
43. P. Dittrich and P. S. Schwille, "Photobleaching and stabilization of fluorophores used for single-molecule analysis with one-and two-photon excitation," Appl. Phys. B **73**(8), 829–837 (2001).
44. Z. Petrmšek and P. Schwille, "Photobleaching in Two-Photon Scanning Fluorescence Correlation Spectroscopy," ChemPhysChem **9**(1), 147–158 (2008).
45. M. Drobizhev, N. S. Makarov, T. Hughes, and A. Rebane, "Resonance enhancement of two-photon absorption in fluorescent proteins," J. Phys. Chem. B **111**(50), 14051–14054 (2007).
46. M. Drobizhev, N. S. Makarov, S. E. Tillo, T. E. Hughes, and A. Rebane, "Two-photon absorption properties of fluorescent proteins," Nat. Methods **8**(5), 393–399 (2011).
47. C. Mätzler, MATLAB Functions for Mie Scattering and Absorption, Institut fur Angewandte Physik: University of Bern (2006).